Atmospheric Chemistry

International Edition: DOI: 10.1002/anie.201510841
German Edition: DOI: 10.1002/ange.201510841

Metastable Nitric Acid Trihydrate in Ice Clouds

*Fabian Weiss, Frank Kubel, Óscar Gálvez, Markus Hoelzel, Stewart F. Parker, Philipp Baloh, Riccardo Iannarelli, Michel J. Rossi, and Hinrich Grothe**

Abstract: *The composition of high-altitude ice clouds is still a matter of intense discussion. The constituents in question are ice and nitric acid hydrates, but the exact phase composition of clouds and its formation mechanisms are still unknown. In this work, conclusive evidence for a long-predicted phase, alpha-nitric acid trihydrate (alpha-NAT), is presented. This phase was characterized by a combination of X-ray and neutron diffraction experiments, allowing a convincing structure solution. Furthermore, vibrational spectra (infrared and inelastic neutron scattering) were recorded and compared with theoretical calculations. A strong interaction between water ice and alpha-NAT was found, which explains the experimental spectra and the phase-transition kinetics. On the basis of these results, we propose a new three-step mechanism for NAT formation in high-altitude ice clouds.*

Nitric acid trihydrate (NAT) is an important constituent of polar stratospheric clouds (PSCs).[1] Balloon-flight[2,3] as well as satellite FTIR measurements accompanied by ground-based LIDAR observed NAT to be present as a mixture with ice.[4] The homogeneous nucleation rates of NAT (upper limit 3×10^{-10} (cm^{-3} air) h^{-1}) are much too low for cloud formation;[5,6] therefore, heterogeneous nucleation on ice or micrometeorites has been proposed.[7,8] The large barrier for homogenous nucleation may be the reason why NAT has never been observed in cloud-chamber experiments, because of a lack of both the time needed for the homogeneous freezing of ice as well as the corresponding nuclei for heterogeneous freezing.[9] In 2004, a research consortium of the National Oceanic and Atmospheric Administration (NOAA) also detected NAT in cirrus clouds and contrails.[10] On the basis of these results and the fact that the amount of water vapor is much too high in these clouds, Gao et al.[11] developed a model that explains, at least theoretically, the high H_2O supersaturation conditions in these high-altitude ice clouds.

Gao et al.[11] suggested that in the upper troposphere (UT), so-called "ice of complex habit" (delta ice) is formed instead of the thermodynamically stable and well-known hexagonal ice. Delta ice was proposed to be a mixture of hexagonal ($P6_3/mmc$) and cubic ice ($Fd\bar{3}m$), although later studies pointed to stacking faults and symmetry reduction,[12,13] and the surface of the solid particles may be covered by NAT. Together, the surface coverage and the metastable phase could suppress the further growth of crystalline particles, which leads to the elevated water vapor pressure observed in field experiments. We surmised that instead of thermodynamically stable beta-NAT, metastable NAT (alpha-NAT) may be formed first, which would explain the results obtained in laboratory and field experiments.

Interestingly, alpha-NAT has not received much attention by atmospheric scientists, and most papers in the field just focus on the thermodynamically stable beta-NAT. However, under the conditions of the lower stratosphere (LS) and the upper troposphere (UT), alpha-NAT can persist for several hours, and when present as a mixture with ice, it can even persist for more than one day.[14] Unfortunately, the crystalline structure of alpha-NAT has not been reported, which has hampered its spectroscopic identification. Spectroscopic data from the laboratory are essential to determine the composition of ice clouds as their analysis relies solely on remote sensing.

Owing to its metastability, it was not possible to grow a single crystal of alpha-NAT, but a pure crystalline powder was accessible. We thus solved the complete structure of alpha-NAT for the first time. When critically comparing the new structure (monoclinic, $P2_1/a$; Figure 1) with the known structure of the beta phase (orthorhombic, $P2_12_12_1$), it becomes obvious that the alpha structure has a lower symmetry but a similar cell volume.[15] However, this structure completely fits both the X-ray and neutron diffraction data, which were independently recorded on samples prepared in the same way (see Figure 2). The refinement was performed with the program package TOPAS 4.2,[16] and the conformities were very high (reliability factors, R_{prof} and wR_{prof}, below 5%). The existence of the alpha-NAT phase has thus been proven by diffraction techniques for the first time.

This newly derived structure was used to calculate its infrared (IR) and inelastic neutron scattering (INS) spectra,

[*] F. Weiss, P. Baloh, Prof. Dr. H. Grothe
Institut für Materialchemie, Technische Universität Wien
Getreidemarkt 9/BC/01, 1060 Wien (Austria)
E-mail: grothe@tuwien.ac.at
Homepage: http://www.imc.tuwien.ac.at
Prof.Dr. F. Kubel
Institut für Chemische Technologie und Analytik
TU Wien (Austria)
Dr. Ó. Gálvez
Instituto de Estructura de la Materia, IEM-CSIC
Madrid (Spain)
Dr. M. Hoelzel
Forschungsneutronenquelle Heinz Maier-Leibnitz (FRM II)
Technische Universität München (Germany)
Dr. S. F. Parker
ISIS Facility, STFC Rutherford Appleton Laboratory
Chilton, Didcot, OX11 0QX (UK)
Dr. R. Iannarelli, Dr. M. J. Rossi
Paul Scherrer Institute, Laboratory for Atmospheric Chemistry
5232 Villigen (Switzerland)
Supporting information and the ORCID identification number(s) for the author(s) of this article can be found under http://dx.doi.org/10.1002/anie.201510841.

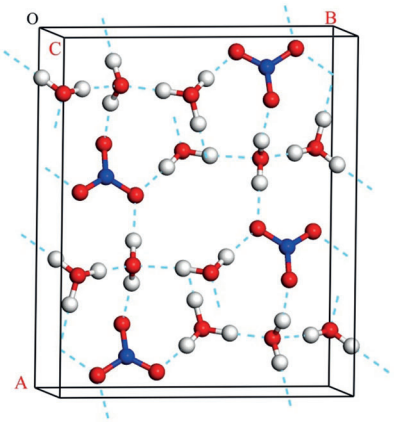

Figure 1. Unit cell of the alpha-NAT structure. Axes: A, B, C (origin O). Oxygen red, nitrogen blue, hydrogen gray. Solid sticks: covalent bonds, dotted lines: hydrogen bonds.

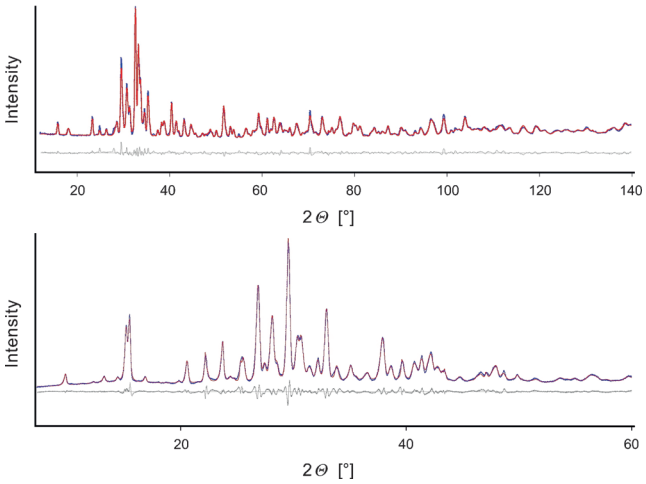

Figure 2. Top: Neutron diffractogram of alpha-NAT generated at 159 K and measured at 4 K. Bottom: X-ray diffractogram of alpha-NAT generated at 155 K. Red: experimental data; blue: calculated data, gray: difference.

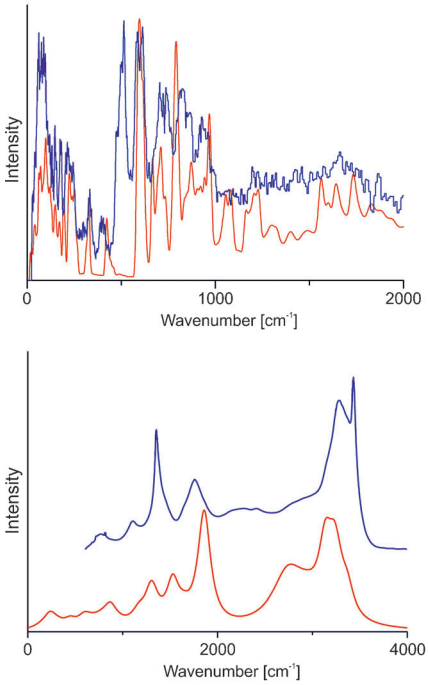

Figure 3. Top: Inelastic neutron scattering of alpha-NAT. Bottom: IR spectra of alpha-NAT. Blue: experimental data, red: data calculated with the CASTEP program package.

which were compared with experimentally recorded ones (see Figure 3). For both spectra, the band positions could be calculated with reasonable accuracy within the limits of such calculations (with harmonic approximation and no model for calculating the width of the IR bands). For the INS spectra, there is missing intensity at 80 and 520 cm^{-1}. These bands can be assigned to the acoustic translations and the librational modes of crystalline ice that are present in all experimental spectra.[17] In the case of the IR spectra (Figure 3, bottom), the calculations again do not provide information about the width of the bands, which were thus arbitrarily represented by Lorentzian functions with a FWHM of 80 cm^{-1} for all wavenumbers except for the OH stretching bands of H_3O^+ (bands at ca. 2900–2700 cm^{-1}), for which a larger width of 200 cm^{-1} was used based on previous studies.[18] Nevertheless, in spite of these limitations, most band positions of the experimental IR spectrum were appropriately reproduced. However, the very narrow band at 3430 cm^{-1}, which appeared as a characteristic pattern in all experimental spectra, did not have significant intensity in the calculations and cannot be attributed to the intrinsic limitations of the theoretical method (see the Supporting Information, Figures S1 and S2, Tables S2a and S2b). We therefore conclude that the observed large intensity of the asymmetric H–O–H stretching vibration in the experimental spectra is an artifact of small crystalline ice clusters introduced at sample preparation.

A possible reason for why we were never able to prepare alpha-NAT in its pure water-free form (as described in the analysis of the vibrational spectra) might be its larger affinity towards water compared to that of beta-NAT, which is due to differences in the structure. To test this hypothesis, we deposited HNO_3 vapor on a pure water ice film at stratospherically relevant temperatures. A deconvolution of the composite IR absorption spectrum revealed that the composite consisted of a mixture of alpha-NAT and pure H_2O ice, but not of beta-NAT, whereas upon annealing, alpha-NAT was finally transformed into beta-NAT.[19] Tables S2a and S2b list the characteristic peak positions of alpha- and beta-NAT that were recorded at 170–190 K and 183–200 K, respectively, in the present work. The growth conditions were chosen to simulate polar stratospheric conditions in terms of temperature (see the Supporting Information).

It should be emphasized that the growth of alpha-NAT occurs without any apparent nucleation barrier under the present conditions when an ice film of sufficient thickness is present. This fact supports the hypothesis made above that the presence of ice stabilizes the metastable alpha-NAT phase. Compared with the concise review of Zondlo et al.,[20] the present results vary in two respects: 1) The formation of a supercooled H_2O/HNO_3 liquid layer before the build-up of

a crystalline alpha-NAT phase, which was observed in several studies, is not observed under our conditions; 2) the evaporation of H_2O from the supercooled liquid H_2O/HNO_3 layer was not necessary to form the crystalline alpha-NAT phase. These observations are in contrast to most published results, as the crystallization of NAT at or below the ice frost point of 188 K had never been observed. Instead, we observed the facile formation of the metastable alpha-NAT phase without an apparent nucleation barrier.[18,19] In earlier kinetic investigations, we had already observed such an interaction between ice and alpha-NAT. Kinetic measurements (using XRD) and cryo-ESEM experiments showed that alpha-NAT crystals are stabilized when incorporated into an ice matrix and survive at much higher temperatures than the pure form.[14]

With the aim of exploring the interaction between NAT and water, we carried out quantum-chemical calculations of the {001} surfaces of alpha- and beta-NAT crystals (for details see the Supporting Information). The calculations predict a larger water adsorption energy (5–30 %) for the surface of alpha-NAT than for beta-NAT, which is in agreement with our hypothesis. Figure 4 shows the adsorption of a six-membered ring of water molecules on a {001} surface of alpha-NAT. Several hydrogen bonds are formed between the water ring and the NAT surface, which provide extra stabilization for alpha-NAT.

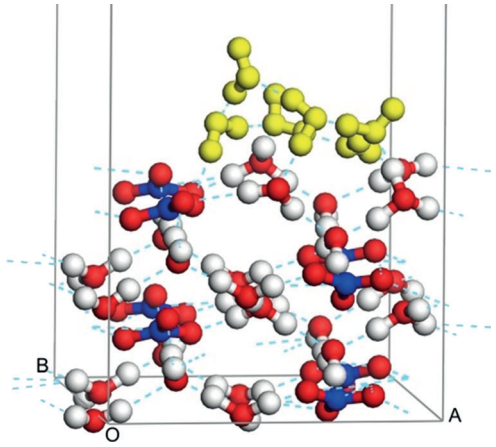

Figure 4. Close-up view of the structure of a water ring on the {001} surface of alpha-NAT. This structure yields the largest adsorption energy (in absolute numbers) for a six-membered ring of water (in yellow) on the {001} surface of alpha-NAT.

The present structure is strongly supported by experiments on alpha-NAT growth monitored by FTIR. HNO_3 was deposited on a thin water ice film (see the Supporting Information for details). The absence of a nucleation barrier at characteristic UT/LS (<188 K) temperatures in the presence of water ice should be emphasized. Furthermore, the conversion of alpha-NAT into stable beta-NAT took place spontaneously under the present experimental conditions (187.5–195 K). We therefore clearly distinguish three phases of NAT growth: 1) formation of alpha-NAT, 2) spontaneous conversion of alpha-NAT into beta-NAT in a narrow temperature window (187.5–195 K), and 3) further growth of beta-NAT up to 195.5 K. In contrast to the reports of Zondlo et al.,[20] but in agreement with earlier work,[21] we did not observe the formation of an amorphous liquid HNO_3/H_2O layer upon the addition of HNO_3 to a pure thin ice film. Therefore, we suggest to modify the PSC Ia formation process by introducing two simplifications: a) The initial formation of an amorphous HNO_3/H_2O liquid is not necessary as metastable alpha-NAT is spontaneously generated in a heterogeneous nucleation process on an ice substrate without a nucleation barrier; and b) crystallization processes occur directly as a result of gas-phase deposition without necessitating slow crystallization processes from the liquid phase. Therefore, alpha-NAT can either form a matrix that embeds crystalline ice particles or be itself embedded inside a matrix of ice.

In conclusion, the formation of NAT in the atmosphere proceeds at $T<188$ K (frost point in UT/LS) via the metastable alpha-NAT phase, which subsequently rearranges to stable beta-NAT upon an increase in temperature. At $T>$ 195 K, alpha-NAT is not observable owing to fast conversion kinetics, and only beta-NAT is observed. The barrier-free growth of alpha-NAT provides strong evidence for the high affinity of NAT towards water ice, which will have to be taken into account in growth scenarios for polar stratospheric clouds in the lower stratosphere and cirrus clouds in the upper troposphere.

Experimental Section

Ostwald's step rule states that in general, it is not the most stable but the least stable polymorph that crystallizes first.[22] This is a tendency observed for the polymorphism of many molecular solids. Starting from a disordered sample (amorphous or supercooled), the least ordered crystalline phase is formed, which is generally metastable. Following this idea, we produced amorphous NAT on a gold-plated support by quenching small droplets (2 μm) generated by a nebulizer (Meinhard TR-50-A1). We were thus able to produce amorphous nitric acid/water samples of various concentrations. Annealing and crystallization gave access to three new metastable hydrate phases,[23] one of which is alpha-NAT at a concentration of 25 mol % (53.8 wt %). The sample amount, however, was always insufficient for high-quality diffraction experiments, which would make the crystalline structure accessible. We solved this problem by spraying directly into liquid nitrogen (77 K). The nebulizer was situated about 30 mm above the liquid surface, allowing rapid heat exchange. Samples produced on the gram scale were investigated by X-ray diffraction, neutron diffraction, and inelastic neutron scattering experiments. After production, the sample was kept at 77 K or below, and the amorphism was confirmed in the corresponding experiments. Subsequently, the sample was annealed above the glass transition point (155 K) to induce the crystallization of the low-temperature polymorph. As the phase transition is irreversible, data collection was started at the lowest temperature possible in the cryostat system. Afterwards, the sample was annealed above the alpha/beta phase-transition temperature (180 K). Again, measurements were carried out at the lowest possible temperature owing to the irreversibility of the phase transition.

The structure of alpha-NAT was computationally modeled using periodic density functional theory with the plane wave pseudopotential method as implemented in the CASTEP code,[25] with a gradient-corrected functional and PBE parametrization[29] employing a plane wave cut-off of 830 eV. This computational method, GGA-PBE, is usually employed for the simulation of molecular solids similar to our

system.[30,31,32] Strict convergence criteria were selected for geometry optimization and the calculation of the vibrational spectra (5×10^{-6} eVatom^{-1}, 0.01 eV Å^{-1}, 0.0001 Å, and 0.02 GPa for energy, maximum force, maximum displacement, and maximum stress, respectively). The experimental structure was relaxed in the geometry optimization process keeping the cell parameters fixed to the measured values.

The INS spectra were recorded using the broadband (0–4000 cm^{-1}) high-resolution spectrometer TOSCA[24] at the ISIS facility. For the calculated INS spectrum of alpha-NAT, we again used the CASTEP code[25] with the parameterization described before. Phonon frequencies were obtained by diagonalization of the dynamic matrix computed using density-functional perturbation theory.[26] The atomic displacements in each mode that are part of the CASTEP output enable the visualization of the modes to aid assignments and are also all that is required to generate the INS spectrum using the program ACLIMAX.[27]

FTIR spectra were recorded by the accumulation of 10 scans at a resolution of 4 cm^{-1} with a Bruker 113v spectrometer for the measurements done at TU Vienna[23] and with a Biorad FTS-575C at PSI.[19]

Neutron diffraction experiments were carried out at the high-resolution powder diffractometer SPODI[28] at the neutron source Heinz Maier-Leibnitz (FRM II) in Garching near Munich, Germany. The data were collected for scattering angles of 0–160° with a step width of 0.05° and a wavelength of 1.5482 Å using a germanium (551) monochromator.

The X-ray diffraction experiments were conducted at the XRC (Vienna University of Technology) with an Xpert Pro Powder Diffractometer (PANalytical) attached to a cryo-stage (Oxford Ltd.). An Xcelerator detector with an active scanning length of 2.122° was used, and measurements were carried out at $Cu_{K\alpha}$ wavelength using a nickel filter.

Acknowledgments

This research project has been supported (in part) by the European Commission under the 7th Framework Program "Strengthening the European Research Area, Research Infrastructures". We acknowledge neutron beam time at ISIS and at the FRM II. The X-ray measurements were carried out within the X-ray Center of the Vienna University of Technology (XRC). H.G. and F.W. are grateful for financial support from the Austria Science Funds (FWF; P23027). O.G. acknowledges financial support from the Ministerio de Ciencia e Innovación ("Ramón y Cajal" program, FIS2010-16455 and CGL2013-48415). R.I. and M.J.R. would like to acknowledge generous funding from the Swiss National Science Foundation (grants 200020_125204 and 200020_144431/1).

Keywords: atmospheric chemistry · diffraction · ice clouds · polar stratospheric clouds · vibrational spectroscopy

[1] S. Solomon, R. R. Garcia, F. S. Rowland, D. J. Wuebbles, *Nature* **1986**, *321*, 755 – 758.
[2] C. Voigt, J. Schreiner, A. Kohlmann, P. Zink, K. Mauersberger, N. Larsen, T. Deshler, C. Kröger, J. Rosen, A. Adriani, F. Cairo, G. Donfrancesco, M. Viterbini, J. Ovarlez, H. Ovarlez, C. David, A. Dörnbrack, *Science* **2000**, *290*, 1756 – 1758.
[3] J. Schreiner, C. Voigt, C. Weisser, A. Kohlmann, K. Mauersberger, T. Deshler, C. Kröger, J. Rosen, N. Kjome, N. Larsen, A. Adriani, F. Cairo, G. Di Donfrancesco, J. Ovarlez, H. Ovarlez, A. Dörnbrack, *J. Geophys. Res.* **2003**, *108*, D58313.
[4] M. Höpfner, N. Larsen, R. Spang, B. P. Luo, J. Ma, S. H. Svendsen, S. D. Eckermann, B. Knudsen, P. Massoli, F. Cairo, G. Stiller, T. V. Clarmann, H. Fischer, *Atmos. Chem. Phys.* **2006**, *6*, 1221 – 1230.
[5] T. Koop, U. M. Biermann, W. Raber, B. P. Luo, P. J. Crutzen, T. Peter, *Geophys. Res. Lett.* **1995**, *22*, 917 – 920.
[6] D. A. Knopf, T. Koop, B. P. Luo, U. G. Weers, T. Peter, *Atmos. Chem. Phys.* **2002**, *2*, 207 – 214.
[7] C. Voigt, H. Schlager, B. P. Luo, A. Dornbrack, A. Roiger, P. Stock, J. Curtius, H. Vossing, S. Borrmann, S. Davies, P. Konopka, C. Schiller, G. Shur, T. Peter, *Atmos. Chem. Phys.* **2005**, *5*, 1371 – 1380.
[8] C. R. Hoyle, I. Engel, B. P. Luo, M. C. Pitts, L. R. Poole, J.-U. Grooß, T. Peter, *Atmos. Chem. Phys.* **2013**, *13*, 9577 – 9595.
[9] O. Stetzer, *Atmos. Chem. Phys.* **2006**, *6*, 3023 – 3033.
[10] P. J. Popp, R. S. Gao, T. P. Marcy, D. W. Fahey, P. K. Hudson, T. L. Thompson, B. Kaercher, B. A. Ridley, A. J. Weinheimer, D. Knapp, D. D. Montzka, D. Baumgardner, T. Garrett, E. Weinstock, J. Smith, D. Sayres, J. Pittman, S. Dhaniyala, T. Bui, M. Mahoney, *J. Geophys. Res. [Atmos.]* **2004**, *109*, D06302.
[11] R. S. Gao, P. J. Popp, D. W. Fahey, T. P. Marcy, R. L. Herman, E. M. Weinstock, D. Baumgardner, T. J. Garrett, K. H. Rosenlof, T. L. Thompson, T. P. Bui, B. A. Ridley, S. C. Wofsy, O. B. Toon, M. A. Tolbert, B. Karcher, T. Peter, P. K. Hudson, A. J. Weinheimer, A. J. Heymsfield, *Science* **2004**, *303*, 516 – 520.
[12] T. L. Malkin, B. J. Murray, A. V. Brukhno, J. Anwar, O. G. Salzmann, *Proc. Natl. Acad. Sci. USA* **2012**, *109*, 1041 – 1045.
[13] W. F. Kuhs, C. Sippel, A. Falenty, T. C. Hansen, *Proc. Natl. Acad. Sci. USA* **2012**, *109*, 21259 – 21264.
[14] H. Grothe, H. Tizek, D. Waller, D. Stokes, *Phys. Chem. Chem. Phys.* **2006**, *8*, 2232 – 2239.
[15] alpha-NAT: ICSD-No.: 426542. beta-NAT: ICSD-No.: 1902.
[16] TOPAS: Version 4.2, Bruker AXS GmbH, Karlsruhe, **2009**.
[17] J. C. Li, *J. Chem. Phys.* **1996**, *105*, 6733 – 6755.
[18] B. M. Llorente, Ph.D. Thesis, **2010**, UAM-CSIC.
[19] R. Iannarelli, M. J. Rossi, *J. Geophys. Res. [Atmos.]* **2015**, 120.
[20] M. A. Zondlo, P. K. Hudson, A. J. Prenni, M. A. Tolbert, *Annu. Rev. Phys. Chem.* **2000**, *51*, 473 – 499.
[21] G. Ritzhaupt, J. P. Devlin, *J. Phys. Chem.* **1991**, 95, 90 – 95.
[22] W. Ostwald, *Z. Phys. Chem.* **1897**, *22*, 289 – 330.
[23] H. Tizek, E. Knözinger, H. Grothe, *Phys. Chem. Chem. Phys.* **2004**, *6*, 972 – 979.
[24] D. Colognesi, M. Celli, F. Cilloco, R. J. Newport, S. F. Parker, V. Rossi-Albertini, F. Sacchetti, J. Tomkinson, M. Zoppi, *Appl. Phys. A* **2002**, *74*, s64 – s66.
[25] S. J. Clark, M. D. Segall, C. J. Pickard, P. J. Hasnip, M. J. Probert, K. Refson, M. C. Payne, *Z. Kristallogr.* **2005**, *220*, 567 – 570.
[26] V. Milman, A. Perlov, K. Refson, S. J. Clark, J. Gavartin, B. Winkler, *J. Phys. Condens. Matter* **2009**, *21*, 485404.
[27] A. J. Ramirez-Cuesta, *Comput. Phys. Commun.* **2004**, *157*, 226.
[28] M. Hoelzel, A. Senyshyn, N. Juenke, H. Boysen, W. Schmahl, H. Fuess, *Nucl. Instrum. Methods Phys. Res.* **2012**, *A667*, 32 – 37.
[29] J. P. Perdew, K. Burke, M. Ernzerhof, *Phys. Rev. Lett.* **1996**, *77*, 3865 – 3868.
[30] B. M. Giuliano, R. M. Escribano, R. Martín-Doménech, E. Dartois, G. M. Muñoz Caro, *A&A* **2004**, *565*, A108.
[31] X. Wu, F. Ma, C. Ma, H. Cui, Z. Liu, H. Zhu, X. Wang, Q. Cui, *J. Chem. Phys.* **2014**, *141*, 024703.
[32] M. Dračínský, M. Šálab, P. Hodgkinson, *CrystEngComm* **2014**, *16*, 6756.

Received: November 23, 2015
Published online: ■■ ■■, ■■■■

Communications

Atmospheric Chemistry

F. Weiss, F. Kubel, Ó. Gálvez, M. Hoelzel, S. F. Parker, P. Baloh, R. Iannarelli, M. J. Rossi, H. Grothe* ____ ▮▮▮▮–▮▮▮▮

Metastable Nitric Acid Trihydrate in Ice Clouds

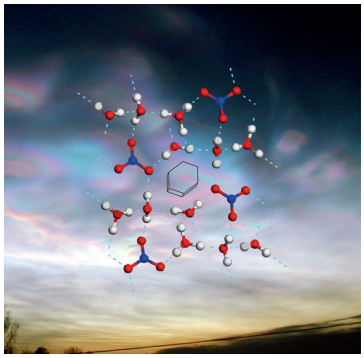

Unknown phase: The structure of nitric acid trihydrate was determined by a combination of X-ray and neutron diffraction experiments and sheds light on the early stages of ice cloud formation in the lower stratosphere and upper troposphere.